DOI: 10.1002/ejic.201000430

Shape Evolution and Tunable Properties of Monodisperse Magnetite Crystals Synthesized by a Facile Surfactant-Free Hydrothermal Method

Rongzheng Liu,[a] Yuzhen Zhao,[a] Rongxia Huang,[a] Yongjie Zhao,[a] and Heping Zhou*[a]

Keywords: Self-assembly / Crystal growth / Surfactant-free / Magnetite / Magnetic properties

Monodisperse Fe_3O_4 crystals have been synthesized by a simple hydrothermal method. Reaction conditions are performed in an ethylene glycol (EG)/NaOH system using $FeCl_3$ as the iron source without adding any surfactants. By adjusting the initial molar ratio of NaOH to Fe^{3+}, several morphologies including solid spheres, hollow spheres, spherical chains, tetrakaidecahedrons, octahedrons, and some flowerlike structures can be obtained. Further investigation reveals that all of the spherical structures are formed by the highly oriented assembly of Fe_3O_4 nanoparticles. The evolution of the morphology from spheres to octahedrons can be attributed to the competition effect between ethylene glycol and NaOH under the reaction conditions. The saturation magnetization, coercivity, and remanent magnetization of the as-synthesized samples vary as the morphology and grain size changes.

Introduction

The controlled synthesis of nanocrystals, which include uniform nanoparticles, and the assembly of architectures by nanoscale building blocks are of fundamental importance for both basic scientific research and practical technological applications. The size and shape of certain monodisperse nanocrystals have a significant effect on their physical and chemical properties, such as their photonic, electronic, magnetic, and catalytic traits.[1–3] Additionally, these shape-controlled nanoparticles can be taken as building blocks for constructing novel self-assembled structures.[4,5] The complex interactions between the building blocks can give rise to extraordinary collective properties.[6] However, development of simple and reliable synthetic methods for nanoparticles, especially the hierarchically self-assembled architectures with controlled morphology and size, is still a challenge.[7]

While shape-controlled studies have been actively pursued on metal and semiconductor nanocrystals,[8–10] only a few studies focus on magnetic iron oxide systems – α-Fe_2O_3,[11] γ-Fe_2O_3,[12] β-FeOOH[13] and Fe_xO-Fe_3O_4.[14] Systematic shape-controlled studies related to magnetite (Fe_3O_4) are rare despite its distinguished role in basic magnetism and technological applications, which include magnetic resonance imaging (MRI),[15] magnetic storage media,[16] ferrofluids,[17] catalysis,[18] and clinical diagnosis and treatment.[19] So far, various Fe_3O_4 structures, such as nanoparticles,[20] spindles,[21] rods,[22] wires,[23] tubes,[24] octahedrons,[25] and nanoparticle assemblies[26] have successfully been fabricated by different methods. Several groups have reported examples for the variable shape of Fe_3O_4 particles by using complex iron sources or various surfactants.[27–29] However, fine shape control of Fe_3O_4 structures through a simple synthesis process with good size and shape-dependent properties remains a difficult task.

In previous studies, monodisperse Fe_3O_4 microspheres and hollow spheres have been synthesized in an ethylene glycol (EG) reaction system using different surfactants and additions [e.g. polyethylene glycol (PEG),[30] dodecylamine (DDA),[31] diethylene glycol (DEG),[32] poly(vinylpyrrolidone) (PVP),[33] oleic acid,[34] ethylenediamine (EDA)[35]] by a hydrothermal method. Although surfactants are necessary in many wet chemical synthesis procedures, they are often adsorbed onto the surface of the formed particles and are difficult to eliminate, which may deteriorate the properties and limit the applications of the final products.[36] As for the Fe_3O_4 particles, the residual surfactants may lead to a low magnetization, which restricts their application in fields requiring a high magnetic field responsiveness.[37] Therefore, the exploration of simple and surfactant-free methods for the preparation of uniform Fe_3O_4 particles with high purity and superior magnetic properties is in demand.

In this study, we present a very simple hydrothermal method for the synthesis of Fe_3O_4 crystals without addition of any surfactant. By adjusting the initial molar ratio of NaOH to Fe^{3+} in the EG reaction system, highly arranged nanoparticle assemblies (e.g. microspheres, hollow spheres, spherical chains, flowerlike spheres) and regular polyhedron particles have been obtained. This surfactant-free prepara-

[a] State Key Laboratory of New Ceramics and Fine Processing, Department of Materials Science and Engineering, Tsinghua University,
Beijing 100084, P. R. China
Fax: +86-10-62772549
E-mail: zhp-dms@tsinghua.edu.cn

Supporting information for this article is available on the WWW under http://dx.doi.org/10.1002/ejic.201000430.

tion method can be assigned as a "green" synthesis route. Furthermore, the evolution of the morphology and grain size can deeply affect the magnetic properties of the products, which reveals tunable properties.

Results and Discussion

Ethylene glycol is a good solvent and a strong reducing agent, which has been widely used in the polyol process to synthesize monodisperse metal or metal oxide crystals.[38,39] Alkaline conditions are also very important in many hydrothermal synthesis procedures, as the free hydroxy groups and the metal ions can combine to form some intermediate compounds, which can then be transformed to the more steady phases in the following reaction process.[40]

Figures 1 and 2 show the low- and high-magnification SEM images of the as-synthesized samples, respectively. With a Fe^{3+} content of 4 mmol and by adjusting the concentration of NaOH, the morphology of the products changes significantly. When the content of NaOH was 0.4 g, solid spheres (Figure 1a) were obtained. By slightly increasing the NaOH content to 0.5 g, the solid spheres transformed into hollow spheres (Figure 1b). High-magnification SEM images reveal that these spherical structures are composed of small nanoparticles (Figure 2a and b). Polyhedron structures appear when the NaOH concentration increases. Figures 1c and 2c show the tetrakaidecahedrons synthesized with a NaOH content of 0.6 g. Some particles of the tetrakaidecahedrons have open pores but maintain the geometry shape (Figure 2d). Uniform and regular octahedrons were obtained when the NaOH content is increased to 0.8 g (Figures 1d and 2e). Both the spherical and polyhedral structures exhibit a very narrow size distribution with average particle sizes of 200 and 150 nm, respectively.

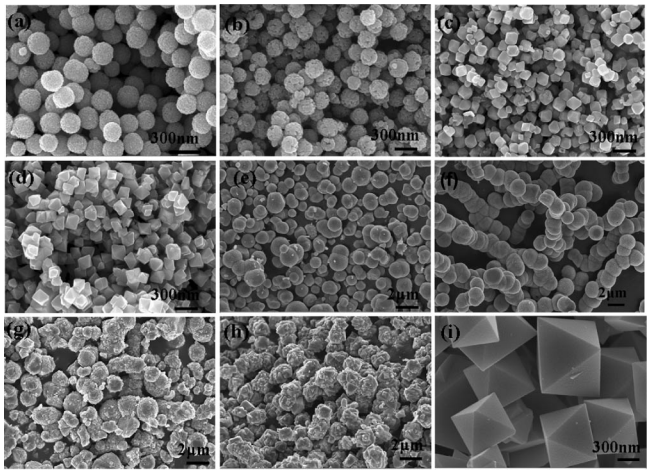

Figure 1. SEM images of the as-synthesized samples: (a) S1, (b) S2, (c) S3, (d) S4, (e) S5, (f) S6, (g) S7, (h) S8, (i) S9.

By decreasing the Fe^{3+} content to 2 mmol and by increasing that of NaOH to 1.0 g, big spheres, as shown in Figure 1e, were fabricated. These micrometer spheres also have interesting subsidiary structures. Many self-assembled

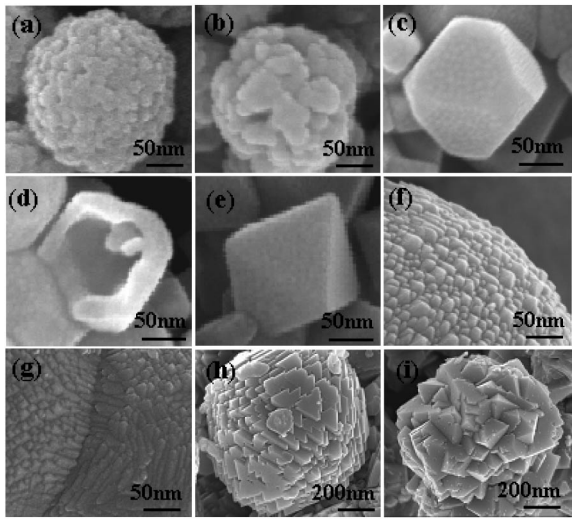

Figure 2. High-magnification SEM images of (a) S1, (b) S2, (c) and (d) S3, (e) S4, (f) S5, (g) S6, (h) S7, (i) S8.

nanoparticles are arranged tightly with relatively close growth directions, as shown in Figure 2f. Further increase in the molar ratio of NaOH/Fe^{3+} to 15 at low Fe^{3+} content values (1 mmol) leads to the formation of spherical chains made up of tens of uniform micrometer spheres. The average lengths of the spherical chains are about 20 μm (Figure 1f). Figure 2g shows the detailed morphology of the junction of two adjacent spheres. The boundary can be seen clearly, and small particles on the two sides of the boundary show symmetrical arrangement directions. The novel morphologies of the big spheres and spherical chains indicate the self-assembly feature of the samples.

At relatively low Fe^{3+} content, when the NaOH content is increased to 1.5 g, flowerlike structures can be obtained (Figure 1g and h). Figure 2h shows the morphology of S7, whose particles keep a nearly spherical shape but composed of regular triangular crystals. Although the triangle crystals are much larger than the subsidiary particles of S5, they are also tightly arranged with special growth directions. When the Fe^{3+} content is further decreased to 1 mmol, the particles consist of even lager crystal structures, which are aggregated together in a spherical shape with an octahedral profile (Figure 2i). These flowerlike structures can be seen as the transition structures from spheres to regular octahedrons. By continuously increasing the alkaline concentration led to irregular particles, but under extremely high alkaline conditions, octahedrons with an average particle size of 800 nm were obtained. All the big octahedrons possess smooth surfaces and clear edges and vertexes (see Figure 1i), which indicates very good crystallinity.

In order to further confirm the effect of the NaOH/Fe^{3+} molar ratio on the morphology of the products, experiments were performed at very high and very low Fe^{3+} concentrations while varying the NaOH content. The results showed that at very high Fe^{3+} content (8 mmol) when the NaOH content was 0.5 g, 1.0 g, and 1.5 g, the shape of the products were solid spheres (50 nm), hollow spheres

(120 nm), and octahedrons (120 nm), respectively (Supporting Information, Figure S1). The particle size becomes smaller at high Fe^{3+} concentrations. At very low Fe^{3+} content values (0.5 mmol), chainlike structures were obtained at various NaOH concentrations. By increasing the NaOH content from 0.5 g to 1.5 g, the building blocks of the chainlike structures change significantly from spheres to octahedrons (Supporting Information, Figure S2).

The morphologies and microstructures of the as-prepared Fe_3O_4 samples were further investigated by transmission electron microscopy (TEM). Figure 3a and c shows the morphologies of the solid spheres and the hollow spheres. For the hollow structures, the subsidiary structures can be seen clearly (inset of Figure 3c). High-resolution TEM (HRTEM) results reveal that the lattice spacing distance is calculated to be 0.485 nm for the solid spheres and 0.296 nm for the hollow spheres, which correspond to the (111) and (220) planes of spinel cubic Fe_3O_4 structure, respectively (Figure 3b and d). Both samples display single crystalline features (inset of Figure 3b and d), which implies that the subcrystals are highly organized. The self-assembled feature of the chainlike structure is also confirmed by TEM images (see Supporting Information, Figure S3). Figure 3e and f shows the morphologies of the big octahedrons. From the inset of Figure 3e it can be seen that the equal-thickness fringes along the edge of the octahedrons reflect a homogeneous incline edge of the octahedrons. The HRTEM image and SAED pattern (Figure 3f) also demonstrate very good crystallinity, and the lattice spacing distance is calculated to be 0.485 nm, which corresponds to the (111) plane of the Fe_3O_4 structure. The bottom right inset of Figure 3f is the amplificatory image of the edge of the octahedron, which clearly reveals that the atoms exhibit a closely packed stacking into a face-centered cubic structure.

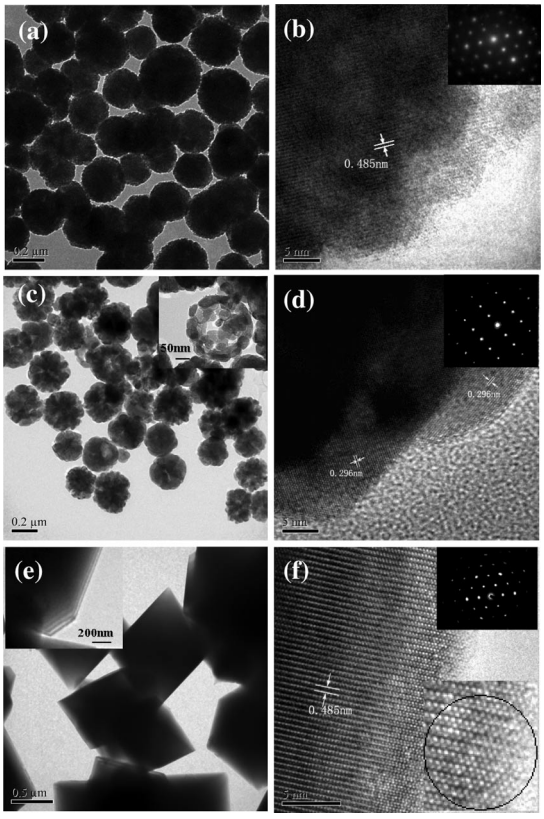

Figure 3. TEM and HRTEM images and the related SAED patterns of: (a) and (b) S1, (c) and (d) S2, (e) and (f) S9. The inset in (c) shows a single particle with open pores. The inset in (e) shows the equal-thickness fringes along the edge of the octahedrons, and the bottom right inset of (f) presents the amplificatory image of the edge of the octahedron.

X-ray diffraction (XRD) is a sophisticated technique used to identify the phase and to study the crystal structure. Figure 4 shows typical XRD patterns of the products. Small spheres (S1), big spheres (S5), hollow spheres (S2), small octahedrons (S4), and big octahedrons (S9) were chosen as the representative samples. All the diffraction peaks can be indexed to the Fe_3O_4 crystals (JCPDS 65–3107) without any impurity phases. In Figure 4d and e, small peaks located at 2θ values of 47.2 and 65.8°can be identified, which can be assigned to the (331) and (531) planes, respectively. The emergence of small peaks represents good crystallinity in the octahedral structures. The full width at half maximum (FWHM) (Figure 4a–e) becomes narrower, which implies that the average grain size decreases. The estimated average grain sizes based on the SEM and TEM results for small octahedrons (S4) and big octahedrons (S9) are about 150 and 800 nm, respectively. For spherical structures composed of subcrystals, the average grain size can be calculated by the Debye–Scherer equation. Calculations based on the (440) peaks reveal that the average grain sizes of the small spheres (S1), big spheres (S5), and hollow spheres (S2) are 13.6, 28.3, and 54.3 nm, respectively.

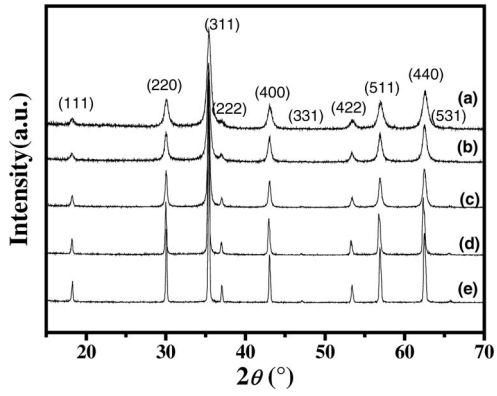

Figure 4. XRD patterns of typical samples: (a) S1, (b) S5, (c) S2, (d) S4, (e) S9.

Energy dispersive X-ray (EDX) spectroscopy was used to determine the elements of the Fe_3O_4 crystals, and the results indicate a very good purity of the samples (see Supporting Information, Figure S4). X-ray photoelectron spectroscopy (XPS) was further applied to identify the composition of the as-synthesized samples. Figure 5a and b shows the spectra of O 1s and Fe 2p core-level peaks of S1 and S9, respectively. In Figure 5a, the major peaks at 529.8 eV for both S1 and S9 are assigned to the lattice oxygen (Fe–O bond) in the Fe_3O_4 products, while the smaller peak with higher

BE for S1 may be assigned to the adsorbed hydroxy group and H_2O of the crystals, which were also identified from the FTIR spectrum (Supporting Information, Figure S5).[41] The photoelectron peaks located at 711.7 and 725.2 eV are the characteristic doublet of the Fe 2p3/2 and Fe 2p1/2 core-level spectra, respectively. The small peak at 55.5 eV was also detected as the characteristic peak of Fe 3p, as shown in the inset of Figure 5b. All the data match well with those of Fe_3O_4 reported in the literature.[42,43]

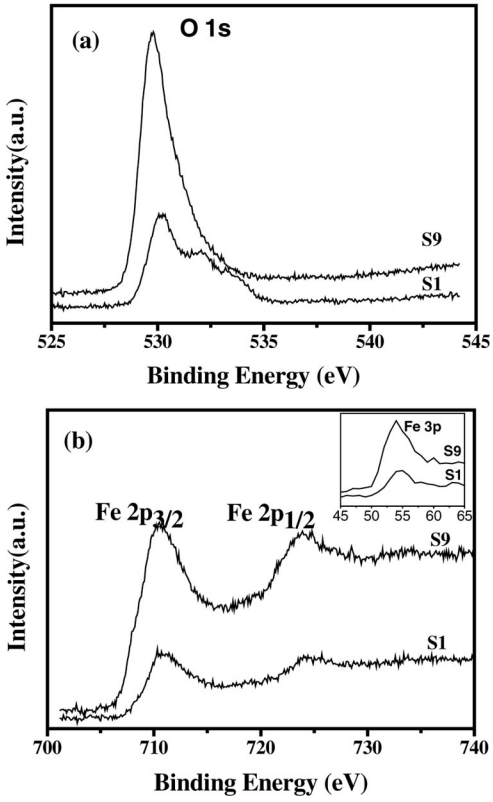

Figure 5. XPS spectra of S1 and S9: (a) O 1s peaks, (b) Fe 2p peaks (inset: Fe 3p peaks).

The results above suggest that it is feasible to tune the shape and grain size of Fe_3O_4 crystals by controlling the initial content of NaOH and Fe^{3+}. In order to further understand the growth mechanism, experiments were carried out at 200 °C for different reaction times. We found that very large and regular hexagonal sheets with an average size of 20 μm and thickness of 600 nm were obtained (Figure 6a) at an earlier stage in the synthesis process of the spherical chains (S6). Some sheets had spherical bumps on the surface, which indicate nucleation of new particles. Thicker and larger flakes were also found at a reaction time of only 30 min for S1 (Supporting Information, Figure S6a). When the reaction time was extended to 60 min, small spherical particles formed on the edge of the flakes (Figure 6b and see Supporting Information, Figure S6b). By further increasing the reaction time to 90 min, a large amount of spheres with some remaining pieces of flakes were obtained as the final products (Figure 6c). The same phenomenon was also seen for the synthesis procedure of S4 at 90 min. Figure 6d reveals that the small polyhedrons stack together and the larger ones separate out. The growth procedures for the big spheres and big octahedrons are different. As for S5 and S9, the original morphologies of the products are similar to those of the final products (Figure 6e and f), and it was difficult to detect any intermediate phase in the earlier formation stage (see Supporting Information, Figure S7).

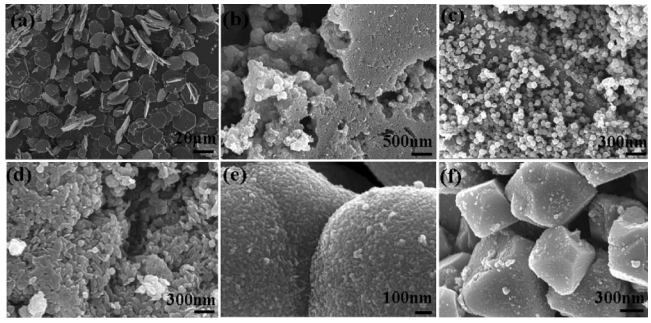

Figure 6. SEM images of the samples at different reaction stages: 60 min for (a) S6 and (b) S1; 90 min for (c) S1, (d) S4, (e) S5, and (f) S9.

The systematic growth mechanism for different samples is illustrated in Figure 7. The control experiments show that the final products are α-Fe_2O_3 with various morphologies when EG is not used under the same reaction conditions (Supporting Information, Figures S8a, S9a–c). A minor amount of Fe_3O_4 mixed in with a predominant amount of polyhedral α-Fe_2O_3 was obtained at low NaOH content with a water/EG ratio of 20/20 mL (Supporting Information, Figures S8b, c, and 9d, e), while under high alkaline conditions, a pure Fe_3O_4 phase was obtained with irregular particle shapes (Supporting Information, Figures S8d, S9f). The results above indicate the important effects of EG and NaOH in the morphology and phase formation of the products. As a good solvent and reducing agent, EG has a significant effect on the spherical morphology of the particles in many hydrothermal synthesis processes. The two hydroxy groups of EG and Fe^{3+} can attach to each other and finally aggregate into spherical structures in isotropic growth directions. At a relatively low NaOH/Fe^{3+} molar ratio, flakelike precursors formed firstly as the intermediate phase, and then a large number of small particles formed as initial crystal nuclei. The as-formed crystal nuclei are unstable and tend to aggregate to form larger Fe_3O_4 spheres through the attachment of the H-bonds of EG and the OH-bonds protruding out of the edge of the nuclei.[44] Because of the greater viscosity of the EG solution, the rate of aggregation of the Fe_3O_4 particles was slow, which provided enough time for the formation of oriented assemblies. Slightly more alkaline conditions can accelerate this process. In the synthesis process of S2, solid spheres were obtained within 2 h (see Supporting Information, Figure S6c, d), which were then transformed into hollow spheres as a result of the Ostwald ripening process.[45] Even lower Fe^{3+} concentrations could lead to chain-like structures, and the formation of this novel structure

might follow an in situ nucleation growth mechanism on the pre-formed hexagonal sheets (see Supporting Information, Figure S6e, f). A detailed formation mechanism of the spherical chains still needs further investigation.

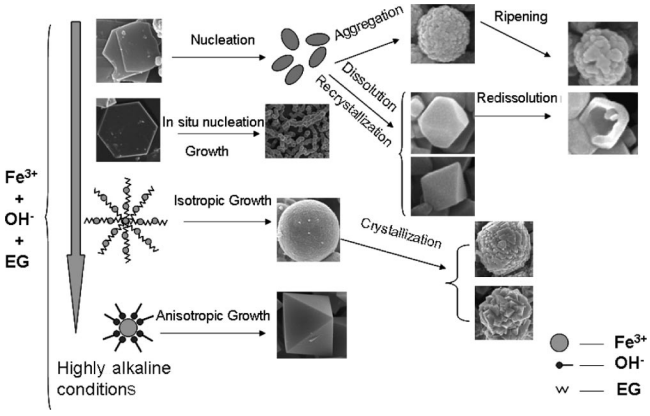

Figure 7. Schematic illustration of the growth mechanism of the as-synthesized samples.

The tetrakaidecahedrons and octahedrons possessed clear vertexes and edges appeared when the NaOH concentration was continuously increased. Under high alkaline conditions, the as-formed small particles have a high solubility and can dissolve again to form more steady structures. As already known, the surface energies of face-centered cubic Fe_3O_4 follow $\gamma\{111\} < \gamma\{100\} < \gamma\{110\}$.[46] Therefore the growth habit determines that the preferred structure is the octahedral structure with eight {111} surfaces exposed outside. The tetrakaidecahedrons with eight {111}, four {110}, and two {100} surfaces can be assigned as the transition structure to the octahedral structure. Some particles with open pores (e.g. S3) can be attributed to the dissolution–recrystallization effect in the growth process, in which large and regular particles form at the expense of small and irregular ones.

At relatively high NaOH concentrations and a low Fe^{3+} content, the growth mechanism is different, as there is no intermediate phase formed as the precursor. In solution, the as-formed magnetite nuclei are attached through the iron atoms with the assistance of the chelating effect of EG. The spheres formed directly from the solution and tend to extend along the radial directions. The flowerlike structures of S7 and S8 maintain the spherical profile, and the low-energy surfaces in the self-assembled regular triangular and octahedral crystals are exposed outside in order to minimize the whole particle surface energy. Under very highly alkaline conditions, abundant free hydroxy groups combine with Fe^{3+} first, and octahedral structures form following the anisotropic growth mode. As no intermediate phase and minor initial nuclei formed, the homogeneous nucleation mechanism can lead to large particle sizes.

Shape evolution reveals that alkaline conditions and the EG reaction conditions have a competitive effect on the shape of the final products, and the obtained morphologies are the result of a balance between the two factors. The isotropic and anisotropic growth modes can lead to spherical and octahedral structures, respectively. Although some mixed morphologies (e.g. polyhedrons with big spheres, irregular spheres, and polyhedrons) (see Supporting Information, Figure S10) have been observed, the particle size changes abruptly from 100–200 nm to 1–2 μm, and it is difficult to see other transitional size magnitudes with uniform morphologies. This might be attributed to thermodynamic factors and different growth mechanisms (e.g. non-homogeneous and homogeneous nucleation mechanisms) under the complex hydrothermal conditions.

The magnetic properties of the as-synthesized samples at room temperature are shown in Figure 8a. All samples exhibit hysteresis loops, which reveal the ferromagnetic features. The main magnetic parameters (e.g. saturation magnetization M_s, coercivity H_c, and remanent magnetization M_r) are significantly affected by the average grain size. Table 1 lists the main magnetic parameters and average grain sizes of typical samples. The influence of the grain size on the saturation magnetization values is evident. The larger the average grain size of the Fe_3O_4 crystal, the higher is the

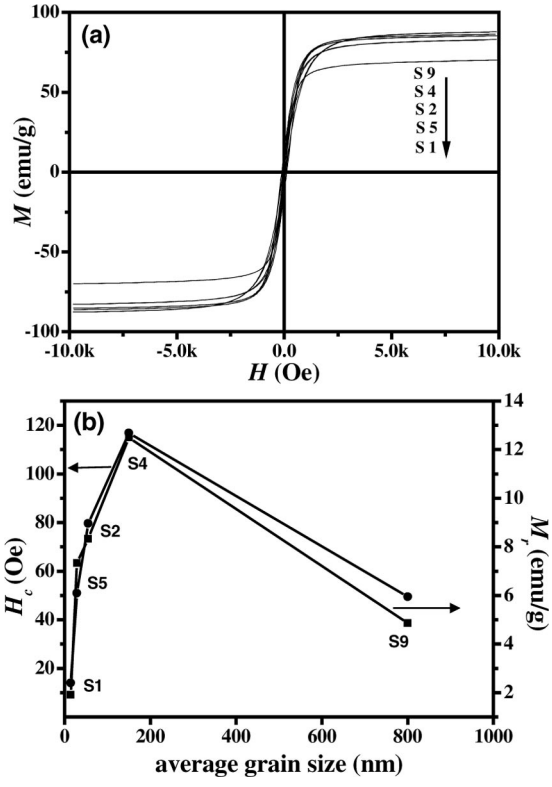

Figure 8. (a) Room-temperature magnetic hysteresis curves of the as-synthesized samples. (b) The coercivity and remanent magnetization as a function of the average grain size.

Table 1. Magnetic properties and the average grain sizes of the as-synthesized samples.

	S1	S5	S2	S4	S9
M_s [emu/g]	70.09	82.95	85.33	86.25	87.77
M_r [emu/g]	1.91	7.33	8.33	12.50	4.86
H_c [Oe]	13.96	50.86	79.62	116.85	49.41
Average grain size [nm]	13.6	28.3	54.3	150	800

saturation magnetization value of the sample. This size effect may be due to the crystallinity of the magnetite particles. The saturation magnetization can be affected by lattice defects, which are more abundant in nanoparticles.[40]

Figure 8b shows the coercivity and remanent magnetization as a function of the average grain size. With increasing grain size, the magnitude of both the coercivity and the remanent magnetization increases and reaches a maximum before dropping again with further increasing grain size. For lager particles, the magnetostatic energy can be decreased by restructuring lager grains into domains. The domain walls can be considered as a transition region across which the direction of magnetization gradually changes. When the size of the particles decreases down to a critical particle diameter, the energy cost of domain formation exceeds the benefits from decreasing the magnetostatic energy and the whole particles tend to become a single domain structure. Since there are no domain walls to move, magnetization reversal in single-domain particles occurs via spin rotation. As it is more difficult to rotate the magnetization than to move a domain wall, single-domain particles have larger coercivity values than those of the multidomain system.[47] When the particle size decreases to a relatively low value, the thermal energy is sufficient to overcome the coupling forces between neighboring atoms, and a transition from ferromagnetic to superparamagnetic then occurs. In this case, the coercivity and the remanent magnetization of the whole sample tend to zero;[48] therefore, the particle size where maximum coercivity occurs corresponds to the size of the single-domain particle.[49] As the remanent magnetization is also deeply affected by the moving of the domain wall and by spin rotation, the evolution trends of the remanent magnetization are similar to those of the coercivity.[50] The variation in the magnetic properties of the as-synthesized Fe_3O_4 samples is well consistent with the theoretical analysis. The magnetic parameters change with grain size, which implies very good tunable properties. These are very important in the application of magnetic materials.

Conclusions

In summary, we have successfully synthesized monodisperse Fe_3O_4 crystals with various morphologies, which include solid spheres, hollow spheres, spherical chains, tetrakaidecahedrons, octahedrons, and some flowerlike structures in the EG/NaOH system without the addition of any surfactants. The morphology evolution from spheres to octahedrons can be attributed to the competitive effect between EG and NaOH under the reaction conditions. The alternating appearance of spherical structures and polyhedral structures with two significantly different particle sizes indicates two different growth mechanisms. The magnetic properties vary as the morphology and the grain size change. With increasing grain size, the saturation magnetization value increases, while the coercivity and the remanent magnetization increase and reach a maximum before dropping again with further increasing grain size. Control of the size and morphology to tailor the chemical and physical properties is also of great significance in other functional material areas. We believe that this facile synthesis process with the EG/NaOH system is extendible to the synthesis of other functional materials.

Experimental Section

All chemicals were of analytical grade and were used as received without further purification. In a typical synthesis procedure, $FeCl_3{\cdot}6H_2O$ (4 mmol) was dissolved in EG (20 mL) under magnetic stirring. NaOH (0.4 g) was then dissolved in EG (20 mL) whilst stirring at 60 °C. The two solutions were mixed together at room temperature to get an even solution. The mixture was transferred into a 50-mL Teflon-lined stainless steel autoclave, sealed, and heated at 200 °C for 10 h. The system was then allowed to cool to room temperature. The black product was collected by centrifuging and by sequentially washing several times with ethanol and deionized water and then dried in a vacuum oven at 60 °C for 4 h. In order to investigate the effect of the initial molar ratio of the reagents, the experimental parameters of other molar ratios of NaOH/Fe^{3+} were also varied out under the same hydrothermal conditions. The detailed synthesis conditions for the preparation of typical samples are listed in Table 2.

The crystal structures of the products were examined by X-ray diffraction (XRD) on a D/max-RB diffractometer by using Cu-K_α radiation (λ = 1.5418 Å). The microstructures were observed with a field emission scanning electron microscope (FESEM, LEO-1530), which was equipped with an energy dispersive X-ray (EDX) spectrometer. TEM (HRTEM) images and corresponding selected area electron diffraction (SAED) patterns were obtained with a JEOL-2011 high-resolution transmission electron microscope (HRTEM, JEOL) at an acceleration voltage of 200 kV. X-ray photoemission

Table 2. Synthesis conditions for the preparation of typical samples.

Sample no.	NaOH [g/mmol]	$FeCl_3$ [mmol]	Molar ratio NaOH/Fe^{3+}	Particle size[a] [nm]	Morphology
S1	0.4/10	4	2.5	200	solid spheres
S2	0.5/12.5	4	3.125	200	hollow spheres
S3	0.6/15	4	3.75	150	tetrakaidecahedrons
S4	0.8/20	4	5.0	150	octahedrons
S5	1.0/25	2	12.5	1500	solid spheres
S6	0.6/15	1	15.0	2000[b]	sphere chains
S7	1.5/37.5	2	18.75	1500	flowerlike spheres
S8	1.5/37.5	1	37.5	2000	flowerlike spheres
S9	3.0/75	2	37.5	800	octahedrons

[a] The particle size was estimated from SEM and TEM observations, which reveal the average level of each sample. [b] The particle size of S6 indicates the average size of the building block units.

spectroscopy (XPS) measurements were carried out with a PHI quantera scanning X-ray microprobe instrument by employing monochromatic Al-Kα radiation as the excitation source. The charge effect was corrected with the adventitious C1s photoelectron signal at 284.8 eV. Fourier transform infrared (FTIR) spectroscopy was performed with a Nicolet 6700 spectrometer. The magnetic properties were investigated with a BHV-50HTI vibrating sample magnetometer (VSM) at room temperature.

Supporting Information (see footnote on the first page of this article): SEM images of the products at different reagent concentrations (Figures S1, S2, and S10) and of typical samples at different times (Figure S6), TEM images of the chainlike structure (Figure S3), FTIR spectrum of S1 (Figure S5), EDX spectrum of the products (Figure S4), photos of the suspensions of the samples prepared at different hydrothermal reaction times (Figure S7), and XRD patterns (Figure S8) and SEM images (Figure S9) of the products without using EG and with a water/EG ratio of 20/20 mL are presented.

Acknowledgments

This work was supported by the National Natural Science Foundation of China (NSFC) (50832003, 50972073). The authors thank Prof. Xiaowen Zhang of Tsinghua University for helpful discussions.

[1] A. P. Alivisatos, K. P. Johnsson, X. G. Peng, T. E. Wilson, C. J. Loweth, M. P. Bruchez, P. G. Schultz, *Nature* **1996**, *382*, 609–611.
[2] X. G. Peng, L. Manna, W. D. Yang, J. Wickham, E. Scher, A. Kadavanich, A. P. Alivisatos, *Nature* **2000**, *404*, 59–61.
[3] X. Wang, J. Zhuang, Q. Peng, Y. Li, *Nature* **2005**, *437*, 121–124.
[4] Y. Huang, X. Duan, Q. Wei, C. Lieber, *Science* **2001**, *291*,630–633.
[5] Z. L. Wang, *J. Phys. Chem. B* **2000**, *104*, 1153–1175.
[6] Z. Y. Tang, N. A. Kotov, *Adv. Mater.* **2005**, *17*, 951–962.
[7] L. S. Zhong, J. S. Hu, *Adv. Mater.* **2006**, *18*, 2426–2431.
[8] Y. G. Sun, Y. N. Xia, *Science* **2002**, *298*, 2176–2179.
[9] A. P. Alivisatos, *Science* **1996**, *271*, 933–937.
[10] S. M. Lee, S. N. Cho, J. Cheon, *Adv. Mater.* **2003**, *15*, 441–444.
[11] X. L. Hu, J. C. Yu, *Adv. Funct. Mater.* **2008**, *18*, 880–887.
[12] J. W. Cheon, N. J. Kang, S. M. Lee, J. H. Lee, J. H. Yoon, S. J. Oh, *J. Am. Chem. Soc.* **2004**, *126*, 1950–1951.
[13] H. Itoh, T. Sugimoto, *J. Colloid Interface Sci.* **2003**, *265*, 283–295.
[14] C. Hofmann, I. Rusakova, T. Ould-Ely, D. Prieto-Centurión, K. B. Hartman, A. T. Kelly, A. Lüttge, K. H. Whitmire, *Adv. Funct. Mater.* **2008**, *18*, 1661–1667.
[15] B. A. Larsen, M. A. Haag, N. J. Serkova, K. R. Shroyer, C. R. Stoldt, *Nanotechnology* **2008**, *19*, 265102–8.
[16] W. Eerenstein, L. Kalev, L. Nieser, T. T. M. Palstra, T. Hibma, *J. Magn. Magn. Mater.* **2003**, *73*, 258–259.
[17] L. Shen, P. E. Laibinis, T. A. Hatton, *Langmuir* **1999**, *15*, 447–453.
[18] Y. Lei, N. W. Cant, D. L. Trimm, *J. Catal.* **2006**, *239*, 227–236.
[19] A. K. Gupta, A. S. G. Curtis, *Biomaterials* **2004**, *25*, 3029–3040.
[20] J. Park, K. An, Y. Hwang, J. G. Park, H. J. Noh, J. Y. Kim, J. H. Park, N. M. Hwang, T. Hyeon, *Nat. Mater.* **2004**, *3*, 891–895.
[21] S. Li, G. W. Qin, W. Pei, Y. Ren, Y. Zhang, C. Esling, L. Zuo, *J. Am. Ceram. Soc.* **2009**, *92*, 631–635.
[22] W. Zhou, K. Tang, S. Zeng, Y. Qi, *Nanotechnology* **2008**, *19*, 065602–10.
[23] L. Y. Zhang, D. S. Xue, X. F. Xu, A. B. Gui, *J. Magn. Magn. Mater.* **2005**, *294*, 10–15.
[24] Y. C. Sui, R. Skomski, K. D. Sorge, D. J. Sellmyer, *Appl. Phys. Lett.* **2004**, *84*, 1525–1527.
[25] C. Hu, Z. Gao, X. Yang, *Chem. Phys. Lett.* **2006**, *429*, 513–517.
[26] J. Zhuang, H. Wu, Y. Yang, Y. C. Cao, *J. Am. Chem. Soc.* **2007**, *129*, 14166–14167.
[27] Q. Dong, N. Kumada, Y. Yonesaki, T. Takei, N. Kinomura, *J. Ceram. Soc. Jpn.* **2009**, *117*, 881–886.
[28] L. Duan, S. Jia, Y. Wang, J. Chen, L. Zhao, *J. Mater. Sci.* **2009**, *44*, 4407–4412.
[29] Y. Y. Zheng, X. B. Wang, L. Shang, C. R. Li, C. Cui, W. J. Dong, W. H. Tang, B. Y. Chen, *Mater. Charact.* **2010**, *61*, 489–492.
[30] H. Deng, X. L. Li, Q. Peng, X. Wang, J. P. Chen, Y. D. Li, *Angew. Chem. Int. Ed.* **2005**, *44*, 2782–2785.
[31] D. Yu, X. Sun, J. Zou, Z. Wang, F. Wang, K. Tang, *J. Phys. Chem. B* **2006**, *110*, 21667–21671.
[32] S. Xuan, Y. X. J. Wang, J. C. Yu, K. C. F. Leung, *Chem. Mater.* **2009**, *21*, 5079–5081.
[33] Y. Zhu, W. Zhao, H. Chen, J. Shi, *J. Phys. Chem. C* **2007**, *111*, 5281–5285.
[34] G. Xi, C. Wang, X. Wang, *Eur. J. Inorg. Chem.* **2008**, *3*, 425–431.
[35] L. P. Zhu, H. M. Xiao, W. D. Zhang, G. Yang, X. Y. Fu, *Cryst. Growth Des.* **2008**, *8*, 957–963.
[36] Y. Shi, S. Peterson, D. Y. Sogah, *Chem. Mater.* **2007**, *19*, 1552–1564.
[37] J. Liu, Z. Sun, Y. Deng, Y. Zou, C. Li, X. Gao, L. Xiong, Y. Gao, F. Li, D. Zhao, *Angew. Chem. Int. Ed.* **2009**, *48*, 1–6.
[38] B. Wiley, T. Herricks, Y. G. Sun, Y. N. Xia, *Nano Lett.* **2004**, *4*, 1733–1739.
[39] D. Larcher, R. J. Partrice, *J. Solid State Chem.* **2000**, *154*, 405–411.
[40] X. Liang, X. Wang, J. Zhuang, Y. T. Chen, D. S. Wang, Y. D. Li, *Adv. Funct. Mater.* **2006**, *16*, 1805–1813.
[41] T. C. Lin, G. Seshadri, J. A. Kelber, *Appl. Surf. Sci.* **1997**, *119*, 83–92.
[42] T. J. Daou, G. Pourroy, S. Bégin-Colin, J. M. Grenèche, C. Ulhaq-Bouillet, *Chem. Mater.* **2006**, *18*, 4399–4404.
[43] X. Teng, D. Black, N. J. Watkins, Y. Gao, H. Yang, *Nano Lett.* **2003**, *3*, 261–264.
[44] S. Li, H. Zhang, Y. J. Ji, D. R. Yang, *Nanotechnology* **2004**, *15*, 1428–1432.
[45] B. Jia, L. Gao, *J. Cryst. Growth* **2007**, *33*, 616–621.
[46] L. Zhang, R. He, C. Gu, *Mater. Res. Bull.* **2006**, *41*, 260–267.
[47] K. J. Klabunde in *Nanoscale Materials in Chemistry*, John Wiley & Sons, Inc., New York, **2001**.
[48] U. Jeong, X. Teng, Y. Wang, H. Yang, Y. Xia, *Adv. Mater.* **2007**, *19*, 33–60.
[49] R. A. Isiam, V. Bedekar, N. Poudyal, J. P. Liu, S. J. Priya, *Appl. Phys.* **2008**, *104*, 104111–4.
[50] E. F. Kneller, F. E. Luborsky, *J. Appl. Phys.* **1963**, *34*, 656–658.

Received: April 19, 2010
Published Online: August 16, 2010

